Micromechanical investigation of particle size effect of granular materials in biaxial test with the role of particle breakage

Pei WANG[1], Zhen-Yu YIN[2] and Zi-Yi WANG[3]

Abstract: Understanding the effect of particle size on the shear strength of granular materials is important for geotechnical design and construction. However, previous studies show contradicting results on the relationship between particle size and shear strength. Besides, the effect of particle breakage on this relationship has not been fully revealed. In this study, a series of biaxial tests have been simulated with DEM to explore the particle size effect of sand considering the role of particle breakage. The sand specimens have parallel particle size distributions. The sequential breakage model has been used to simulate particle breakage, which is a combination of replacement and cluster methods. The main conclusions of this study are: (1) the relationship of peak shear strength and particle size depends on the crushability of particles and relative density of specimens; (2) the particle size and crushability have a very slight effect on the residual shear strength; (3) at the microscale, the relationship of shear strength and particle size is positively related to the friction utilization ratio.

Keywords: particle size effect; granular media; particle breakage; discrete element method; crushability

---

[1] Postdoctoral Fellow, Department of Civil and Environmental Engineering, The Hong Kong Polytechnic University, Hung Hom, Kowloon, Hong Kong, China. Email: pei-cee.wang@polyu.edu.hk

2 Associate Professor. Department of Civil and Environmental Engineering, The Hong Kong Polytechnic University, Hung Hom, Kowloon, Hong Kong, China (Corresponding author). Tel: (+852) 3400 8470, Fax: (+852) 2334 6389; Email: zhenyu.yin@polyu.edu.hk; zhenyu.yin@gmail.com

[3] Research Assistant, Department of Civil and Environmental Engineering, The Hong Kong Polytechnic University, Hung Hom, Kowloon, Hong Kong, China. Email: wangziyi970325@gmail.com

Introduction

The mechanical behavior of granular materials is closely related to the characteristics of particles, such as size, shape, crushability, and packing (Jin et al. 2018; Kawamoto et al. 2018; Wang and Arson 2018; Xiao et al. 2019; Yang et al. 2018; Zhang et al. 2020; Zhou et al. 2013). Understanding the effect of these characteristics on the macroscopic behavior of granular materials is of significant importance for their engineering applications (Jin et al. 2016; Jin et al. 2018; Wang and Yin 2020; Yin et al. 2018; Zhang et al. 2019). It is well-acknowledged that particle size plays an important role in determining the macroscopic behavior of granular materials, which is called the particle size effect.

The effect of particle size on the macroscopic shear strength, as a fundamental issue of granular materials, has been extensively studied. Marsal (Marsal 1967) conducted a series of large-scale triaxial tests (specimens 113 cm in diameter) on three different rockfill materials which have parallel gradations. And he found that the specimen with a larger mean particle size has a lower shear strength. Later, Marschi *et al.* (1972) also performed triaxial tests on rockfill materials of different sizes. Different from Marsal's tests, Marschi *et al.* adjusted the size of specimens so that the ratio of maximum particle size and specimen size was fixed for all tests. The results showed that the peak shear strength decreases with the increase of particle size, and they proposed that the particle size effect is due to the increased amount of particle breakage in specimens with larger particles. This finding was later simulated and verified in (Hu et al. 2018; Yin et al. 2017). In the true triaxial tests on rockfill materials by Xiao *et al.* (Xiao et al. 2014), the friction angle was found to decrease with the increase of particle size. Results from other studies indicated that the particle breakage decreases the shear strength and is a source of particle size effect (Daouadji et al. 2001; Frossard et al. 2012; Lade and Bopp 2005). However, in some other studies, the opposite conclusion on the effect of particle size, i.e. the shear strength increases with the increase of particle size, was reported. Gupta found that the internal friction angle of the river bed material increases with the increase of particle size. However, when he replaced the river bed material with blasted material, this angle decreases with particle size (Gupta 2016). Islam et al. (Islam et al. 2019) conducted a series of direct shear tests on particle samples with particle size ranging from 0.075 mm to 1.18 mm, and they found that both the shear strength and internal friction angle increase with the increase of particle size. Other studies (Alias et al. 2014; Cao et al. 2020) also stated that both the peak and residual shear strengths increase with particle size. The particle size effect was also investigated using the discrete element method (DEM) (Cil et al. 2020). Results showed that the peak shear strength increases with the increase of particle size while the residual strength is not affected by particle size (Jiang et al. 2018; Sitharam and Nimbkar 2000). In these simulations, however, particles were assumed uncrushable. To sum up, although efforts have been made to investigate the effect of particle size on the shear strength of granular materials, no consensus has been made reached on this issue. In addition, the influence of particle breakage on the size effect is still not clear.

The objective of this study is to investigate the particle size effect with the role of particle breakage. To achieve this goal, a series of biaxial tests are simulated with DEM on sand specimens of different particle sizes and reference tensile strengths. The flexible boundary imposed by the latex membrane in experiments is modeled by the flexible-bonded particle approach. The soil particles are crushable, and the crushing process obeys the sequential breakage model proposed by one of the authors (Wang et al. 2019). The macroscopic behavior in the biaxial tests with different particle sizes are compared and analyzed. In addition, particle breakage and its effect on shear strength are discussed in depth from micro to macro.

DEM simulation of biaxial test considering particle breakage

Particle breakage is a common phenomenon in civil engineering, pharmaceutical industry, and mineral industry (Chen et al. 2020; Coop et al. 2004; Wang and Arson 2016; Wang and Yin 2020; Zhou et al. 2019). In a granular assembly, particle breakage occurs when the internal stress of a particle exceeds the material's strength. Particle breakage plays an important role in determining the properties and behaviors of granular materials, such as internal friction angle, permeability, yielding stress, volume change, etc. (Karatza et al. 2019; Lade et al. 1996; Shahnazari and Rezvani 2013; Yin et al. 2020). In recent years, the X-ray micro-computed tomography (X-μCT), which allows the characterization of particle size, shape, movement and interaction nondestructively, has been widely used in the analysis of particle breakage (Seo et al. 2020; Zhao et al. 2020). The high-resolution images from X-μCT have been successfully employed to identify broken particles, classify broken modes, and provide realistic particle shapes of fragments, and significantly expanded our knowledge on the micro-mechanisms of particle breakage (Alikarami et al. 2015; Druckrey and Alshibli 2016; Karatza et al. 2018). Despite its advantages in producing realistic and quantitative data of particle breakage, it is still challenging for X-μCT to obtain the contact forces within a granular assembly, which play an important role in the determination of particle breakage. On the other hand, DEM could easily calculate the contact force between particles according to contact laws, and simulate the movement and breakage of particles. Another advantage of DEM is that it is very convenient to control the mechanical properties of soil particles (such as particle strength in this study), which significantly increases the controllability and repeatability of the virtual experiments. Therefore, the DEM is adopted in this study to analyze the particle size effect.

In the DEM model in this study, biaxial tests are simulated with sand specimens with a dimension of 9.7 mm×2.34 mm×18 mm. The specimens are prepared with the isotropic compression method, and the flexible-bonded particle approach is used to simulate the rubber membrane in the experiment (Zhang et al. 2020). The model prameters were previously calibrated against the experimental results of biaxial tests on sand specimens by Alshibli and Sture (Alshibli and Sture 2000). Good agreement was achieved between the simulation results and experimental observation. Detailed information about the specimen preparation and calibration can be found in the Appendix of this paper. A summary of the DEM parameters used in the biaxial simulations is shown in Table 1.

In DEM, two common methods to simulate particle breakage are the cluster method and replacement method. In the cluster method, crushable particles are represented by bonded elements (usually elementary spheres), and particle breakage is simulated by the bond breakage. In this method, micro-cracks occur in a particle before a major breakage event and can be tracked by the number of broken bonds. The shape of fragments truly depends on the stress distribution in the crushable particle, but precise models are usually computationally expensive due to a large number of spheres in each cluster. In addition, the initial porosity of a specimen made of clusters is much higher than experimental measurements due to the internal voids. In the replacement method, once a particle breaks, it is replaced by several smaller fragments (Cil and Buscarnera 2016). The replacement method is more effective because the number of particles in DEM is equal to the number of soil particles. The size, shape and arrangement of fragments are often related to the contact forces and positions of the mother particle, and must be specified in the replacement model. And the conservation of mass and energy are also important considerations during the replacement.

The breakage model presented in Figure 1 is used for this study, which is a combination of cluster and replacement methods. This model was proposed by the authors in a previous study of particle breakage in oedometer test (Wang et al. 2019). Based on the sequential breakage mechanism characterized from XCT images of oedometer tests with zeolite particles, this breakage model could simulate particle breakage of multiple generations with two different breakage modes, i.e. the particle splitting modeled by replacement method and the comminution modeled by bond breakage. In the first generation, the particle splits into two fragments once the maximum normal contact force reaches a threshold. Each fragment has a roughly hemispherical shape with 17 balls bonded with parallel bonds, as shown in Figure 1. The 17 balls are inscribed in the mother particle to minimize the mass (volume) loss in the replacement. The breakage plane is determined by the directions of principal stresses and the position of the contact with maximum normal force. In the following generations, breakage can be simulated with either replacement method or cluster method depending on the maximum normal contact force and stresses within parallel bonds. The mass loss is an important consideration in the replacement method, and previous studies show that it doesn't have a strong influence on simulation results when it is below a critical value, i.e. 47% according to Ciantia *et al.* (2015). A common assumption of the volume loss is that it is formed by fine particles generated during the breakage which have a small influence on the macroscopic mechanical behavior. The mass loss in the breakage model in Figure 1 is 46%, which is below the critical value. It is also important to mention that the internal voids within fragments account for a large portion of the mass loss, which has a very slight effect on the soil behavior. At last, it is also important to mention that there is also some energy loss in the replacement process, which does not have a significant effect on the simulation results under the quasi-static loading condition. As proved by many researchers, in a single particle crushing test, the strength of a particle increases when the particle size decreases (McDowell and Bolton 1998; Wang and Arson 2016). To account for this effect, the Weibull theory is adopted in this model to predict the strength for particles and parallel bonds of various sizes. To sum up, compared to previous breakage models, the current model has high computational efficiency without a large number of elementary balls at the beginning; considers multiple generations of breakage under both splitting and comminution modes; contains non-spherical fragments made of bonded spherical particles. A detailed description of the failure mechanism and breakage model can be found in (Wang et al. 2019).

The main micro-mechanical parameters associated with the breakage model are the reference tensile strength in the Weibull theory (σ_{t0}), the Weibull modulus (m), the normal and shear bond strengths ($\bar{\sigma}_c$ and $\bar{\tau}_c$), the parallel bond normal and shear stiffnesses ($\bar{k}_n$ and $\bar{k}_s$). In this study, σ_{t0} represents the tensile strength of the particle with d =1 mm, and it ranges from 1.5 to 2.5 MPa in different tests to simulate particles with various crushability. Weibull modulus is chosen as 4.5 according to experimental results (Lobo-Guerrero and Vallejo 2006). Both $\bar{\sigma}_c$ and $\bar{\tau}_c$ are assumed to follow the Weibull theory with the same σ_{t0} and m of soil particles. The equivalent normal and shear stiffness, $\pi R^2 \bar{k}_n$ and $\pi R^2 \bar{k}_s$, are also equal to the stiffness of soil particles. In order to reduce the computation cost, the smallest breakable particle size is set as 0.175 mm, which enables a maximum replacement generation of two. Particles below this size threshold are often excluded from force chains (Desu and Annabattula 2019), and have a very slight effect on the shear strength when they account for less than 20% total weight according to Habib et al. (Taha et al. 2019).

In this study, 32 biaxial tests are simulated with the above-mentioned sample preparation method and breakage model, which are summarized in Table 2. Both loose and dense specimens are simulated with d_{50} ranging from 0.22 to 0.55 mm are prepared. The following macro- and micro-mechanical analysis focus on the test results from S1 to S16 with the lower and upper bounding particle sizes of 0.22 and 0.55 mm. And tests S17 to S32 show similar behaviors. Parallel particle size distributions (PSDs) are used in the DEM simulations, in which cumulative particle weight curves are parallel to each other with different d_{50}. With this method, each d_{50} corresponds to a specific PSD with a known shape for the cumulative particle weight curve. Therefore, for a given d_{50}, the DEM simulation could focus on the effect of particle size with an otherwise similar PSD. Besides crushable particles, uncrushable particles (σ_{t0} equal to infinity) are also used in some tests for comparison.

Particle size effect

Particle size effect on shear strength

Figure 2 shows the evolution of principal stress ratio (σ_1 / σ_3) and volumetric strain with axial strain in the biaxial tests. In general, typical shear behaviors in experiments are successfully reproduced in the numerical tests. The tests with dense specimens exhibit obvious post-peak strain-softening behavior, while loose specimens only show hardening behavior. In terms of the volume change, tests with dense specimens slightly contract at first and then experience continuous dilation. Note that to main a constant particle volume in calculating the void ratio, the volume loss is simplified as virtual fine particles whose positions are assumed to be the same with the fragments generated from the same mother particle. With otherwise similar conditions, tests with dense specimens tend to have larger volumetric strains than the loose ones. The effect of particle breakage is obvious. As the reference tensile strength σ_{t0} decreases from 2.5 MPa to 1.5 MPa (increase crushability), the peak shear strength significantly decreases in coarse specimens ($d_{50} = 0.55$ mm). As a result, the post-peak strain softening behavior becomes milder in tests S2 and S3 compared with that in tests S1, and even disappears in tests S4, as shown in Figure 2(a). On the other hand, the effect of σ_{t0} on the shear behaviors of specimens with $d_{50} = 0.22$ mm is much less evident. When σ_{t0} is decreases, there is a very slight decrease in peak shear strength for the dense specimens (Figure 2(c)). For the loose specimens, peak and residual shear strengths remain stable regardless of particle crushability (Figure 2(g)). This result can be attributed to the low crushability for fine particles. Previous studies show that the strengths of sand particles follow the Weibull statistics, and large particles are more vulnerable to breakage due to lower tensile strengths (Huang et al. 2020; Wang and Arson 2016). In the biaxial tests in this study, the percentage of crushed particles is higher in specimens with $d_{50} = 0.55$ mm than that in specimens with $d_{50} = 0.22$ mm, which is consistent with the results from previous studies and explains the significant decrease of peak shear strength for coarse particles with the increase of particle crushability. The detailed information on particle breakage during the biaxial tests will be presented in the next subsection.

The peak and residual stress ratios in the biaxial tests are summarized in Figure 3(a) and (b) respectively for the dense and loose specimens. It is evident from the figures that particle breakage plays an important role in determining the shear strength. For the dense specimens in Figure 3(a), the peak stress ratio increases with the increase of particle size when there is no/very slight particle breakage (uncrushable particles or particles with σ_t =2.5 MPa and 2.0 MPa). However, when the particle crushability is high (σ_t =1.5 MPa), the peak stress ratio decreases with the increase of particle size. On the other hand, the particle breakage has a very low effect on the residual shear strength. In Figure 3(a), tests with different particle crushability (σ_t) exhibit a similar residual stress ratio, and this ratio slightly increases with particle size. This result is consistent with another study in which a relatively stable residual state was found for tests with different particle crushability (Ma et al. 2016). In terms of loose specimens in Figure 3(b), the peak and residual stress ratios are similar because there is no shear band formation. In addition, both peak and residual stress ratios slightly increase with the increase of particle size, despite the difference in particle crushability. In other words, the particle size effect is very mild in loose specimens.

Evolution of particle breakage

Particle breakage has a strong influence on the shear strength of granular materials, and it is often deemed as the reason for the particle size effect (Daouadji et al. 2001; Hassanlourad et al. 2008; Xiao et al. 2014). To illustrate this mechanism, the evolution of particle breakage in the biaxial tests with different particle sizes and reference tensile strengths are presented and discussed.

Figure 4 and Figure 5 show the particle displacement and crushed particles in dense specimens at the end of shearing (tests S1 and S5 are not presented due to no particle breakage). It can be seen from the figures that the sand specimens are separated into several blocks with distinct particle displacements, and inter-particle shear movement mainly happens at the interface between the contacting blocks. The interfaces between these blocks have strong localization of shear deformation and are usually called shear bands (Alshibli and Sture 1999; Zhu and Yin 2019). Different types of shear bands are observed in the tests, such as parallel band in S2 and S3, reflected band in S4, diagonal band in S6 and S7, and X-shaped band in S8. It is worth noting that all these patterns of shear bands are common in experiments (Desrues and Viggiani 2004), and the difference comes from the various microscopic imperfections in the specimens. Particle breakage occurs in all the tests, but the number and locations of crushed particles are strongly affected by the reference tensile strength σ_{t0}. In general, the number of crushed particles increases with the decrease of σ_{t0}. In tests S2 and S6 with σ_{t0} equal to 2.5 MPa, the percentages of crushed particles are very low and no obvious region of concentration of crushed particles can be identified. As σ_{t0} decreases to 2.0 MPa (tests S3 and S7), the number of crushed particles is increased and the crushed particles tend to concentrate in the regions of shear bands. A further decrease of σ_{t0} to 1.5 MPa significantly increases the number of crushed particles, as shown by the results of tests S4 and S8 respectively in Figure 4(c) and Figure 5(c).

The particle displacement and crushed particles in loose specimens, i.e. tests S10 to S12 are presented in Figure 6. Note that because tests S14 to S16 show similar evolution patterns with tests S10 to S12, their results are not repeated here. Different from the failure pattern in dense specimens in Figure 4 and Figure 5, no obvious shear band can be observed in the loose specimens. In addition, the lateral expansion of loose specimens is much milder than the dense ones. The positions of crushed particles are randomly distributed in the whole specimen, compared with those concentrated within in the shear band for dense specimens. As expected, the number of crushed particles increases with the decrease of the reference tensile strength. In addition, extensive particle breakage occurs near the top and bottom loading platens, see Figure 6(c). This phenomenon is in agreement with experimental observations in (Karatza et al. 2019; Tsoungui et al. 1999), which can be explained by the lower coordination number for the particles near the loading platen (Wang and Arson 2016).

The evolutions of particle breakage ratio (number of crushed particles/ number of total particles) and bond breakage ratio (number of broken bonds/ number of total bonds) with axial strain in different tests are summarized in Figure 7. The particle breakage ratio describes the percentage of particles that are subjected to splitting failure. For dense specimens in Figure 7(a) and (b), the particle breakage ratio increases rapidly at the early stage of shearing until reaching a peak stress ratio. In the post-peak softening stage, particle breakage ratio continues to increase but at a slower rate. While for the loose specimens in Figure 7(c) and (d), the breakage ratio increases with vertical strain in an almost linear pattern. The final breakage ratio is very sensitive to the reference tensile strength of particles. For example, the final breakage ratio increases by around 500% with σ_{t0} decreasing from 2.5 MPa in S10 to 1.5 MPa in S12. In addition, the particle size also has a strong influence on the final breakage ratio. Compared the results from coarse specimens in Figure 7(a) with those from fine specimens in Figure 7(b), the increase of particle size results in a significant increase in the particle breakage ratio. Besides the splitting failure, the comminution is also one of the important failure modes of sand particles (Seo et al. 2020) and can be qualitatively characterized by the bond breakage ratio (Harireche and McDowell 2003). In all the tests in Figure 7(e) to (h), the bond breakage ratios increase rapidly at the beginning of tests, and soon reach a relatively stable value until the end of the tests. In other words, the percentage of particles subjected to comminution failure remains almost constant during the test. In addition, similar to the particle breakage ratio, the bond breakage ratio also increases with the decrease of σ_{t0}. Note that because a particle may have several bonds within a cluster, a bond breakage does not guarantee the generation of new fragments. It is well-known that particle breakage is always accompanied by volumetric compression (Coop et al. 2004; Lade et al. 1996), and therefore a specimen with higher breakage ratio and bond breakage ratio usually has a lower shear strength.

Besides the particle breakage ratio, the position of particle breakage is also important because the shear failure of a crushable granular material is often associated with the breakage concentration within the shear band. The crushed particles at different loading strains in test S8 are shown in Figure 8. At the very early stage of shearing ($\varepsilon_{zz} = 1\%$), only a small amount of particles are crushed, which are randomly distributed within the specimen. At the peak state ($\varepsilon_{zz} = 3\%$), an increased number of particles are crushed, as shown in Figure 8(b). Due to the particle breakage, strong force chains cannot develop within the specimen. Therefore, specimens with a low reference tensile strengths (σ_{t0}) usually have a reduced peak strength. At this stage, although the number of crushed particles accounts for more than 50% of the final crushed particles at the end of the test, there is no obvious breakage concentration. In the post peak stage, as the vertical strain continues to increase, particle breakage starts to concentrate in the two diagonal directions forming an X-shape shear band. At this stage, because the deformation of the specimen mainly localizes in the shear band region, the shear resistance is dominated by the interparticle shear force at the interface. As the vertical strain continues to increase from 10% to 15%, almost all breakage happens within the shear band.

The particle size distributions at different stages in dense specimens are presented in Figure 9. In all the tests, as the strain increases, particles continue to break, generating smaller particles and increasing fine contents. At the same time, the distributions move leftward due to the reduction of large particles. Similar shift patterns of distribution curves are often observed in tests with crushable granular materials (Einav 2007; Wei et al. 2018). As the reference tensile strength decreases from 2.5 MPa to 1.5 MPa, an obvious increase of fine content can be observed. It is worth mentioning that to avoid high computational cost the minimum particle size is set as 0.022 mm.

Micromechanical analysis

In this section, the particle size effect will be further investigated at the microscale. Because the failure and shear strength of a specimen is closely related to the development of shear band, the location of shear band should be determined first. In this study, the grain rotation based method proposed by one of the authors is adopted to identify the shear band (Zhu and Yin 2019). In this method, particles with high rotation are determined based on the particle rotation distribution $\beta_v(\omega)$, which is defined as the volumetric percentage of particles with a rotation angle larger than ω in a small loading increment. And the zone with a concentration of high rotation particles is the location of shear band. Figure 10 shows the evolution of void ratio inside shear band along with vertical strain for dense specimens. In order to obtain the void ratio inside shear band, a number of measure spheres are placed within shear band, and the average measured void ratio is adopted. Note that loose specimens are not showing because no shear band is generated in biaxial tests with loose specimens. As shown in Figure 10, void ratios in different specimens are similar at the beginning, and then start to diverge at the vertical strain of 3%. With otherwise similar conditions, the specimen with uncrushable particles yields the highest void ratio inside shear band. The final void ratio decreases with the decrease of particle strength. The results are reasonable as the voids among large particles are filled with fines produced by breakage. Similar results that particle breakage decreases the dilation of granular materials is also reported in (Ghafghazi et al. 2014; Yu 2017). Therefore, the volumetric dilation of shear band, which is induced by the rearrangement of particles and contributes to the shear strength, is weakened by particle breakage. In terms of the particle size effect, the final void ratio increases with the increase of particle size when σ_{t0} is high, such as 0.815 for S5 and 0.84 for S1. However, when the particles are weak and vulnerable to breakage, the final void ratio decreases with particle size, such as 0.79 for S8 and 0.77 for S4. This relationship is consistent with the macroscopic volume change in Figure 2.

Previous studies showed that the coordination number is closely related to the particle breakage, and particles with a high coordination number are more resistive to breakage (Lim and McDowell 2007). Figure 11 shows the evolutions of coordination number in tests S1 and S3. Before shearing, the coordination number is around 5.1 for particles inside and outside of shear band. For both tests with uncrushable (S1) and crushable (S3) particles, the coordination number decreases significantly at the beginning of shearing and then becomes stable. The decrease of the coordination number can be explained by the dilation of the dense specimens during the biaxial shear tests. As expected, particles inside the shear band have a lower coordination number compared to particles outside. In addition, particles in test S3 have a higher average coordination number than that in S1 due to particle breakage. According to

Figure 7(a) and 7(c), extensive particle breakage happens with the vertical strain ranging from 0.01 to 0.05 in test S3, which corresponds to a coordination number in the range from 4.0 to 4.4. This observation is in agreement with previous studies based on XCT that splitting and fragmentation are the dominant modes when the coordination number is less than 5.6 (Karatza et al. 2019). In other tests, the evolutions of coordination number are similar and the particle size shows a very slight effect on the coordination number.

According to previous studies, the interparticle friction force plays an important role in the shear resistance of granular material, and the specimen with a larger interparticle friction coefficient tends to have higher shear strength (Antony and Kruyt 2009; Huang et al. 2014; Yang et al. 2012). Therefore, the friction utilization ratio, u_{UR}, is proposed here to investigate the relationship between interparticle friction force and shear strength. The friction utilization ratio is defined as the ratio of current interparticle shear force (F_s) and maximum shear force ($F_{s\_\max}$). With the linear contact model in this study, $F_{s\_\max}$ is given as μF_n, where F_n is the interparticle normal force. For a sand specimen, particle contacts have different u_{UR} depending on their stress states. A specimen with a higher average u_{UR} usually indicates that stronger resistance to particle movement and rearrangement, and thus has a higher shear strength. The probability density functions of friction utilization ratio and the average ratio of all contacts are shown in Figure 12. It is clear from the figure that although the specimens have different particle sizes and reference tensile strengths, they share a similar distribution for the friction utilization ratio. From Figure 12(a), the u_{UR} decreases with the decrease of reference tensile strength of particles, indicating a lower percentage of shear resistance capacity has been used to resist the external loads. As a result, the peak shear also decreases with a low reference tensile strength of particles. Compare the results in Figure 12(a) and (b), when the mean particle size increases from 0.22 to 0.55 mm, u_{UR} also increases in tests with low particle crushability

(S5 versus S1, S6 versus S2, and S7 versus S3). While in test S4 and S8 with high particle crushability, u_{UR} decreases with the increase of particle size. This relationship is consistent with the relationship between particle size and peak stress ratio in Figure 3. For the loose specimens in Figure 12(c) and (d), the u_{UR} is always lower than those of the corresponding dense specimens. Therefore, loose specimens have lower peak strengths than the corresponding dense specimens.

Conclusions

In this study, a series of biaxial tests have been conducted with DEM to explore the particle size effect of sand. The soil particles are crushable, and the crushing process obeys the sequential breakage model proposed by one of the authors (Wang et al. 2019). The shear strength in tests with different particle sizes and reference tensile strengths have been compared and analyzed. Then the evolution of particle breakage and its relationship with shear strength has been discussed. Finally, the micro-mechanical analysis in terms of void ratio inside shear band and interparticle shear force has been conducted. The main conclusions of this study are:

(1) For a granular assembly, the relationship of peak shear strength and particle size depends on the crushability of particles and the relative density of specimens. The shear strength of a dense specimen increases with the increase of particle size when particles are uncrushable or strong (have a high reference tensile strength). On the other hand, when the crushability of particles is high, the shear strength decreases with the increase of particle size. In addition, the particle size effect is very mild in loose specimens.

(2) The particle size and crushability have a very slight effect on the residual shear strength of granular material. After shearing, the residual strengths of both loose and dense specimens are similar, despite of the obvious differences in particle size, relative density, and crushability.

(3) At the microscale, the relationship of shear strength and particle size is positively related to the friction utilization ratio. The friction utilization ratio generally describes to what extent the capacity to resist interparticle sliding is utilized. This ratio generally increases with the increase of particle size, which results in an increasing peak shear strength. However, when there is extensive particle breakage, the friction utilization ratio as well as peak strength decrease with the increase of particle size.

Data Availability Statement

All data, models, or code that support the findings of this study are available from the corresponding author upon reasonable request.

Acknowledgement

The financial support provided by the GRF project (Grant No. 15209119, R5037-18F) from the Research Grants Council (RGC) of Hong Kong is gratefully acknowledged.

Appendix: Calibration of DEM samples and parameters

DEM Samples

The schematic diagram of the model for biaxial tests is shown in Figure A1(a). The PSDs in DEM simulations and experiments are shown in Figure A1(b), with average particle sizes of

0.22 mm and 0.55 mm respectively for F-sand and M-sand. The method proposed by Wood and Maeda (Wood and Maeda 2008) to calculate the maximum and minimum void ratios in 2D is slightly modified to account for the 3D condition in this study. Firstly, a large number of randomly generated particles are subjected to an isotropic compression of 100 kPa with the inter-particle friction coefficient equal to 0.0. Once the system becomes stable, the inter-particle friction coefficient is changed to the final value (0.5) and then the DEM calculation starts again. After the system reaches equilibrium, the current void ratio of the specimen is determined as the minimum void ratio (e_{min}). Similarly, the loosest specimen with the maximum void ratio (e_{max}) can be generated in the same way with the inter-particle friction coefficient set as 1.0 during the initial isotropic compression. Then the DEM model for biaxial test is prepared as follows: (1) particle generation at specified relative density; (2) isotropic compression until a target confining pressure of 100 kPa; (3) flexible boundary replacement according to the flexible-bonded particle approach (Zhang et al. 2020).

After the generation process, the specimen is sheared by moving the top and bottom walls towards the specimen, and the constant confining pressure is kept by applying forces to the membrane particles. The membrane is made of equal-sized particles with simple cubic packing, and the radii of these particles are 0.11 mm. The overlap between contacting particles is 0.5 times the radius, i.e. 0.0505 mm. To avoid the soil particles puncturing the flexible membrane, a high value is chosen for both the tensile and shear strengths of the parallel bonds. The magnitude of force applied to a membrane particle is the product of the equivalent area of the particle and the confining pressure. The forces applied to the membrane particles are continuously adjusted during the simulation to account for an evolving equivalent area. For the two walls in the Y direction, their positions are fixed to provide a plane strain condition. The test stops when the axial strain reaches 15%.

DEM Parameters

The DEM model was calibrated against the results of biaxial tests by Alshibli and Sture (Alshibli and Sture 2000). The calibrated parameters will be briefly introduced in the following. The particle density ρ is chosen as 2650 kg/m^3, which is close to natural sands. The normal and shear stiffness of particles, k_n and k_s, are 5×10^7 N/m to guarantee that the average overlap ratio, defined as the ratio of overlap length and particle diameter, is lower than 1%. Note that the linear contact model with a fixed stiffness rather than the nonlinear elastic model is adopted for this study, because the bulk behavior of granular materials is qualitatively similar with either model according to the comparisons made by the authors and Ji *et al.* (2006). The friction coefficient of soil particles, u, is chosen as 0.5 as a rule of thumb. In order to consider the particle shape of sand particles in the experiments, the rolling resistance method is adopted for soil particles. Rather than physically approximating the angular particles with clusters or clumps, the rolling resistance method is a numerical method to simulate the non-spherical particles (Ai et al. 2011; Yang et al. 2017). In this method, a rotational torque is applied to resist the rolling at the contact to account for the interlocking between the two contacting angular particles. The rolling resistance coefficient (μ_r), contact effective radius ($\bar{R}$), and normal contact force (F_n) determine the maximum limiting value of the toque as $\mu_r \bar{R} F_n$. Previous studies showed that this method is able to reproduce both macro- and microscopic behaviors of granular material with a coefficient smaller than 0.3, beyond which the mechanical properties remains almost the same (Liu et al. 2018; Zhao et al. 2018). In this study, the calibrated μ_r for the particle-particle and particle-wall contacts are respectively 0.15 and 0.0. The values of μ_r do not change during the tests, and the particle shape evolution is ignored for simplicity. It is also assumed that μ_r at the particle-wall contact is 0.0. The stiffness of the parallel bond, $\bar{k}_n$ and $\bar{k}_s$, are set as 1.0×10^{10} N/m^3, so that the equivalent normal and shear stiffness, given by $\pi R^2 \bar{k}_n$ and $\pi R^2 \bar{k}_s$, are much lower than soil particles. The tensile and shear strengths of parallel bonds are 1.0×10^{27} N/m^2, which is high enough to avoid soil particles puncturing the flexible membrane. A summary of the DEM parameters used in the biaxial simulations is shown in Table 1.

The macroscopic behaviors from DEM simulation and experiments are shown in Figure A1(c) and (d). For both dense and medium dense specimens, the DEM simulations and experiments have a reasonable good match in terms of the evolutions of principal stress ratio and volumetric strain.

References

Ai, J., Chen, J. F., Rotter, J. M., and Ooi, J. Y. (2011). "Assessment of rolling resistance models in discrete element simulations." *Powder Technol*, 206(3), 269-282. https://doi.org/10.1016/j.powtec.2010.09.030

Alias, R., Kasa, A., and Taha, M. R. (2014). "Particle size effect on shear strength of granular materials in direct shear test." *Int. J. Civil. Env. Struct. Constr. Archit. Eng*, 8(11), 733-736. https://doi.org/10.5281/zenodo.1096805

Alikarami, R., Andò, E., Gkiousas-Kapnisis, M., Torabi, A., and Viggiani, G. (2015). "Strain localisation and grain breakage in sand under shearing at high mean stress: insights from in situ X-ray tomography." *Acta Geotech*, 10(1), 15-30. https://doi.org/10.1007/s11440-014-0364-6

Alshibli, K. A., and Sture, S. (1999). "Sand shear band thickness measurements by digital imaging techniques." *Journal of computing in civil engineering*, 13(2), 103-109. https://doi.org/10.1061/(ASCE)0887-3801(1999)13:2(103)

Alshibli, K. A., and Sture, S. (2000). "Shear band formation in plane strain experiments of sand." *J Geotech Geoenviron*, 126(6), 495-503. https://doi.org/10.1061/(Asce)1090-0241(2000)126:6(495)

Antony, S. J., and Kruyt, N. P. (2009). "Role of interparticle friction and particle-scale elasticity in the shear-strength mechanism of three-dimensional granular media." *Phys Rev E*, 79(3). https://doi.org/10.1103/PhysRevE.79.031308

Cao, P., Jiang, M.-j., and Ding, Z.-j. (2020). "Effects of particle size on mechanical behaviors of calcareous sand under triaxial conditions." *Japanese Geotechnical Society Special Publication*, 8(5), 182-187. https://doi.org/10.3208/jgssp.v08.c54

Chen, W.-B., Liu, K., Yin, Z.-Y., and Yin, J.-H. (2020). "Crushing and Flooding Effects on One-Dimensional Time-Dependent Behaviors of a Granular Soil." 20(2), 04019156. https://doi.org/10.1061/(ASCE)GM.1943-5622.0001560

Ciantia, M. O., Arroyo, M., Calvetti, F., and Gens, A. (2015). “An approach to enhance efficiency of DEM modelling of soils with crushable grains.” *Geotechnique*, 65(2), 91-110. https://doi.org/10.1680/geot.13.P.218

Cil, M. B., and Buscarnera, G. (2016). “DEM assessment of scaling laws capturing the grain size dependence of yielding in granular soils.” *Granul Matter*, 18(3). https://doi.org/10.1007/s10035-016-0638-9

Cil, M. B., Sohn, C. B., and Buscarnera, G. (2020). “DEM Modeling of Grain Size Effect in Brittle Granular Soils.” *J Eng Mech*, 146(3). https://10.1061/(Asce)Em.1943-7889.0001713

Coop, M. R., Sorensen, K. K., Freitas, T. B., and Georgoutsos, G. (2004). “Particle breakage during shearing of a carbonate sand.” *Geotechnique*, 54(3), 157-163. https://doi.org/10.1680/geot.2004.54.3.157

Daouadji, A., Hicher, P.-Y., and Rahma, A. (2001). “An elastoplastic model for granular materials taking into account grain breakage.” *European Journal of Mechanics - A/Solids*, 20(1), 113-137. https://doi.org/10.1016/S0997-7538(00)01130-X

Desrues, J., and Viggiani, G. (2004). “Strain localization in sand: an overview of the experimental results obtained in Grenoble using stereophotogrammetry.” *Int J Numer Anal Met*, 28(4), 279-321. https://doi.org/10.1002/nag.338

Desu, R. K., and Annabattula, R. K. (2019). “Particle size effects on the contact force distribution in compacted polydisperse granular assemblies.” *Granul Matter*, 21(2), 29. https://doi.org/10.1007/s10035-019-0883-9

Druckrey, A. M., and Alshibli, K. A. (2016). “3D finite element modeling of sand particle fracture based on in situ X-Ray synchrotron imaging.” *Int J Numer Anal Met*, 40(1), 105-116. https://doi.org/10.1002/nag.2396

Einav, I. (2007). “Breakage mechanics - Part I: Theory.” *J Mech Phys Solids*, 55(6), 1274-1297. https://doi.org/10.1016/j.jmps.2006.11.003

Frossard, E., Hu, W., Dano, C., and Hicher, P. Y. (2012). “Rockfill shear strength evaluation: a rational method based on size effects.” *Geotechnique*, 62(5), 415-427. https://doi.org/10.1680/geot.10.P.079

Ghafghazi, M., Shuttle, D. A., and DeJong, J. T. (2014). “Particle breakage and the critical state of sand.” *Soils Found*, 54(3), 451-461. https://doi.org/10.1016/j.sandf.2014.04.016

Gupta, A. K. (2016). “Effects of particle size and confining pressure on breakage factor of rockfill materials using medium triaxial test.” *Journal of Rock Mechanics and Geotechnical Engineering*, 8(3), 378-388. https://doi.org/10.1016/j.jrmge.2015.12.005

Harireche, O., and McDowell, G. R. (2003). “Discrete element modelling of cyclic loading of crushable aggreates.” *Granul Matter*, 5(3), 147-151. 10.1007/s10035-003-0143-9

Hassanlourad, M., Salehzadeh, H., and Shahnazari, H. (2008). “Dilation and particle breakage effects on the shear strength of calcareous sands based on energy aspects.” *Int J Civ Eng*, 6(2), 108-119. https://doi.org/10.1179/1938636213Z.00000000050

Hu, W., Yin, Z.-Y., Scaringi, G., Dano, C., and Hicher, P.-Y. (2018). “Relating fragmentation, plastic work and critical state in crushable rock clasts.” *Eng Geol*, 246, 326-336. https://doi.org/10.1016/j.enggeo.2018.10.012

Huang, Q. S., Zhou, W., Ma, G., Ng, T. T., and Xu, K. (2020). “Experimental and numerical investigation of Weibullian behavior of grain crushing strength.” *Geoscience Frontiers*, 11(2), 401-411. https://doi.org/10.1016/j.gsf.2019.07.007

Huang, X., Hanley, K. J., O'Sullivan, C., and Kwok, C. Y. (2014). “Exploring the influence of interparticle friction on critical state behaviour using DEM.” *Int J Numer Anal Met*, 38(12), 1276-1297. https://doi.org/10.1002/nag.2259

Islam, M. N., Siddika, A., Hossain, M. B., Rahman, A., and Asad, M. A. (2019). “Effect of particle size on the shear strength behavior of sands.” *arXiv preprint arXiv:1902.09079*.

Ji, S., and Shen Hayley, H. (2006). “Effect of Contact Force Models on Granular Flow Dynamics.” *J Eng Mech*, 132(11), 1252-1259. 10.1061/(ASCE)0733-9399(2006)132:11(1252)

Jiang, M. D., Yang, Z. X., Barreto, D., and Xie, Y. H. (2018). “The influence of particle-size distribution on critical state behavior of spherical and non-spherical particle assemblies.” *Granul Matter*, 20(4), 80. https://doi.org/10.1007/s10035-018-0850-x

Jin, Y.-F., Yin, Z.-Y., Shen, S.-L., and Hicher, P.-Y. (2016). “Investigation into MOGA for identifying parameters of a critical-state-based sand model and parameters correlation by factor analysis.” *Acta Geotech*, 11(5), 1131-1145. https://doi.org/10.1007/s11440-015-0425-5

Jin, Y.-F., Yin, Z.-Y., Wu, Z.-X., and Daouadji, A. (2018). “Numerical modeling of pile penetration in silica sands considering the effect of grain breakage.” *Finite Elem Anal Des*, 144, 15-29. https://doi.org/10.1016/j.finel.2018.02.003

Jin, Y. F., Yin, Z. Y., Wu, Z. X., and Zhou, W. H. (2018). “Identifying parameters of easily crushable sand and application to offshore pile driving.” *Ocean Eng*, 154, 416-429. https://doi.org/10.1016/j.oceaneng.2018.01.023

Karatza, Z., Ando, E., Papanicolopulos, S. A., Ooi, J. Y., and Viggiani, G. (2018). “Evolution of deformation and breakage in sand studied using X-ray tomography.” *Geotechnique*, 68(2), 107-117. 10.1680/jgeot.16.P.208

Karatza, Z., Ando, E., Papanicolopulos, S. A., Viggiani, G., and Ooi, J. Y. (2019). “Effect of particle morphology and contacts on particle breakage in a granular assembly studied using X-ray tomography.” *Granul Matter*, 21(3). https://doi.org/10.1007/s10035-019-0898-2

Kawamoto, R., Ando, E., Viggiani, G., and Andrade, J. E. (2018). “All you need is shape: Predicting shear banding in sand with LS-DEM.” *J Mech Phys Solids*, 111, 375-392.

Lade, P. V., and Bopp, P. A. (2005). “Relative density effects on drained sand behavior at high pressures.” *Soils Found*, 45(1), 1-13. https://doi.org/10.3208/sandf.45.1_1

Lade, P. V., Yamamuro, J. A., and Bopp, P. A. (1996). “Significance of particle crushing in granular materials.” *Journal of Geotechnical Engineering-Asce*, 122(4), 309-316. https://doi.org/10.1061/(Asce)0733-9410(1996)122:4(309)

Lim, W. L., and McDowell, G. R. (2007). “The importance of coordination number in using agglomerates to simulate crushable particles in the discrete element method.” *Geotechnique*, 57(8), 701-705. 10.1680/geot.2007.57.8.701

Liu, Y. M., Liu, H. B., and Mao, H. J. (2018). “The influence of rolling resistance on the stress-dilatancy and fabric anisotropy of granular materials.” *Granul Matter*, 20(1). 10.1007/s10035-017-0780-z

Lobo-Guerrero, S., and Vallejo, L. E. (2006). “Application of Weibull statistics to the tensile strength of rock aggregates.” *J Geotech Geoenviron*, 132(6), 786-790. https://doi.org/10.1061/(ASCE)1090-0241(2006)132:6(786)

Ma, G., Zhou, W., Chang, X. L., Ng, T. T., and Yang, L. F. (2016). “Formation of shear bands in crushable and irregularly shaped granular materials and the associated microstructural evolution.” *Powder Technol*, 301, 118-130. https://doi.org/10.1016/j.powtec.2016.05.068

Marsal, R. J. (1967). “Large scale testing of rockfill materials.” *Journal of the Soil Mechanics and Foundations Division*, 93(2), 27-43. https://doi.org/10.1061/JSFEAQ.0000958

Marschi, N. D., Chan, C. K., and Seed, H. B. (1972). “Evaluation of properties of rockfill materials.” *Journal of the Soil Mechanics and Foundations Division*, 98(1), 95-114. https://doi.org/10.1061/JSFEAQ.0001735

McDowell, G. R., and Bolton, M. D. (1998). “On the micromechanics of crushable aggregates.” *Geotechnique*, 48(5), 667-679. https://doi.org/10.1680/geot.1998.48.5.667
Seo, D., Sohn, C., Cil, M. B., and Buscarnera, G. (2020). “Evolution of particle morphology and mode of fracture during the oedometric compression of sand.” *Geotechnique*, 0, 1-13. https://doi.org/10.1680/jgeot.18.P.300
Shahnazari, H., and Rezvani, R. (2013). “Effective parameters for the particle breakage of calcareous sands: An experimental study.” *Eng Geol*, 159, 98-105. https://doi.org/10.1016/j.enggeo.2013.03.005
Sitharam, T. G., and Nimbkar, M. S. (2000). “Micromechanical modelling of granular materials: effect of particle size and gradation.” *Geotechnical & Geological Engineering*, 18(2), 91-117. https://doi.org/10.1023/A:1008982027109
Taha, H., Nguyen, N.-S., Marot, D., Hijazi, A., and Abou-Saleh, K. (2019). “Micro-scale investigation of the role of finer grains in the behavior of bidisperse granular materials.” *Granul Matter*, 21(2), 28. https://doi.org/10.1007/s10035-019-0867-9
Tsoungui, O., Vallet, D., and Charmet, J. C. (1999). “Numerical model of crushing of grains inside two-dimensional granular materials.” *Powder Technol*, 105(1-3), 190-198. https://doi.org/10.1016/S0032-5910(99)00137-0
Wang, P., and Arson, C. (2016). “Discrete element modeling of shielding and size effects during single particle crushing.” *Comput Geotech*, 78, 227-236. https://doi.org/10.1016/j.compgeo.2016.04.003
Wang, P., and Arson, C. (2018). “Energy distribution during the quasi-static confined comminution of granular materials.” *Acta Geotech*, 13(5), 1075-1083. https://doi.org/10.1007/s11440-017-0622-5
Wang, P., Karatza, Z., and Arson, C. (2019). “DEM modelling of sequential fragmentation of zeolite granules under oedometric compression based on XCT observations.” *Powder Technol*, 347, 66-75. https://doi.org/10.1016/j.powtec.2019.02.050
Wang, P., and Yin, Z.-Y. (2020). “Micro-mechanical analysis of caisson foundation in sand using DEM.” *Ocean Eng*, 203, 107240. https://doi.org/10.1016/j.oceaneng.2020.107240
Wang, P., and Yin, Z.-Y. (2020). “Micro-mechanical analysis of caisson foundation in sand using DEM: Particle breakage effect.” *Ocean Eng*, 215, 107921. https://doi.org/10.1016/j.oceaneng.2020.107921
Wei, H. Z., Zhao, T., He, J. Q., Meng, Q. S., and Wang, X. Z. (2018). “Evolution of Particle Breakage for Calcareous Sands during Ring Shear Tests.” *Int J Geomech*, 18(2). https://doi.org/10.1061/(Asce)Gm.1943-5622.0001073
Wood, D. M., and Maeda, K. (2008). “Changing grading of soil: effect on critical states.” *Acta Geotech*, 3(1), 3-14. https://doi.org/10.1007/s11440-007-0041-0
Xiao, Y., Liu, H., Chen, Y., and Zhang, W. (2014). “Particle size effects in granular soils under true triaxial conditions.” *Geotechnique*, 64(8), 667-672. https://doi.org/10.1680/geot.14.T.002
Xiao, Y., Long, L., Matthew Evans, T., Zhou, H., Liu, H., and Stuedlein Armin, W. (2019). “Effect of Particle Shape on Stress-Dilatancy Responses of Medium-Dense Sands.” *J Geotech Geoenviron*, 145(2), 04018105. https://doi.org/10.1061/(ASCE)GT.1943-5606.0001994
Yang, Y., Cheng, Y. M., and Sun, Q. C. (2017). “The effects of rolling resistance and non-convex particle on the mechanics of the undrained granular assembles in 2D.” *Powder Technol*, 318, 528-542. https://doi.org/10.1016/j.powtec.2017.06.027
Yang, Y., Cheng, Y. M., and Sun, Q. C. (2018). “Revisiting the confined comminution of granular materials with the consideration of the initial particle size distributions and

repetitive loadings." *Powder Technol*, 329, 149-157. https://doi.org/10.1016/j.powtec.2018.01.045

Yang, Z. X., Yang, J., and Wang, L. Z. (2012). "On the influence of inter-particle friction and dilatancy in granular materials: a numerical analysis." *Granul Matter*, 14(3), 433-447. https://doi.org/10.1007/s10035-012-0348-x

Yin, Z.-Y., Hicher, P.-Y., Dano, C., and Jin, Y.-F. (2017). "Modeling mechanical behavior of very coarse granular materials." *J Eng Mech*, 143(1), C4016006. https://doi.org/10.1061/(ASCE)EM.1943-7889.0001059

Yin, Z.-Y., Wang, P., and Zhang, F. (2020). "Effect of particle shape on the progressive failure of shield tunnel face in granular soils by coupled FDM-DEM method." *Tunn Undergr Sp Tech*, 100, 103394. https://doi.org/10.1016/j.tust.2020.103394

Yin, Z.-Y., Wu, Z.-X., and Hicher, P.-Y. (2018). "Modeling monotonic and cyclic behavior of granular materials by exponential constitutive function." *J Eng Mech*, 144(4), 04018014. https://doi.org/10.1061/(ASCE)EM.1943-7889.0001437

Yu, F. (2017). "Particle breakage and the drained shear behavior of sands." *Int J Geomech*, 17(8), 04017041. https://doi.org/10.1061/(ASCE)GM.1943-5622.0000919

Zhang, F., Li, M., Peng, M., Chen, C., and Zhang, L. (2019). "Three-dimensional DEM modeling of the stress–strain behavior for the gap-graded soils subjected to internal erosion." *Acta Geotech*, 14(2), 487-503. https://doi.org/10.1007/s11440-018-0655-4

Zhang, J., Wang, X., Yin, Z.-Y., and Liang, Z. (2020). "DEM modeling of large-scale triaxial test of rock clasts considering realistic particle shapes and flexible membrane boundary." *Eng Geol*, 279, 105871. https://doi.org/10.1016/j.enggeo.2020.105871

Zhang, Y., Zhou, X., and Wen, Y. (2020). "Constitutive Theory for Sand Based on the Concept of Critical Fabric Surface." *J Eng Mech*, 146(4), 04020019. https://doi.org/10.1061/(ASCE)EM.1943-7889.0001741

Zhao, B., Wang, J., Andò, E., Viggiani, G., and Coop, M. R. (2020). "Investigation of particle breakage under one-dimensional compression of sand using X-ray microtomography." *Can Geotech J*, 57(5), 754-762. https://doi.org/10.1139/cgj-2018-0548

Zhao, S. W., Evans, T. M., and Zhou, X. W. (2018). "Shear-induced anisotropy of granular materials with rolling resistance and particle shape effects." *Int J Solids Struct*, 150, 268-281. 10.1016/j.ijsolstr.2018.06.024

Zhou, W., Ma, G., Chang, X. L., and Zhou, C. B. (2013). "Influence of Particle Shape on Behavior of Rockfill Using a Three-Dimensional Deformable DEM." *J Eng Mech*, 139(12), 1868-1873. https://doi.org/10.1061/(Asce)Em.1943-7889.0000604

Zhou, X., Ma, G., and Zhang, Y. (2019). "Grain size and time effect on the deformation of rockfill dams: a case study on the Shuibuya CFRD." *Geotechnique*, 69(7), 606-619. https://doi.org/10.1680/jgeot.17.P.299

Zhu, H. X., and Yin, Z. Y. (2019). "Grain Rotation-Based Analysis Method for Shear Band." *J Eng Mech*, 145(10). https://doi.org/10.1061/(ASCE)EM.1943-7889.0001654

Tables

Table 1. Parameters used in DEM simulations

Particle type	Parameters	Values
Soil particle	Density ρ (kg/m^3)	2650
	Normal and shear stiffness k_n and k_s (N/m)	5×10^7
	Frictional coefficient u (-)	0.5
	Rolling resistant coefficient μ_r (-)	0.15
Membrane particle	Density ρ (kg/m^3)	800
	Normal and shear stiffness of parallel bond $\bar{k}_n$ and $\bar{k}_s$ (N/m^3)	1.0×10^{10}
	Frictional coefficient u (-)	0.0
	Normal and shear strength of parallel bond $\bar{\sigma}_c$ and $\bar{\tau}_c$ (N/m^2)	1.0×10^{27}

Table 2. Summary of biaxial tests conducted with DEM

Test name	d_{50} (mm)	σ_{t0} (MPa)	Relative density	Test name	d_{50} (mm)	σ_{t0} (MPa)	Relative density
S1	0.55	∞	89.0%	S17	0.30	∞	89.0%
S2	0.55	2.5	89.0%	S18	0.30	2.5	89.0%
S3	0.55	2.0	89.0%	S19	0.30	2.0	89.0%
S4	0.55	1.5	89.0%	S20	0.30	1.5	89.0%
S5	0.22	∞	89.0%	S21	0.40	∞	89.0%
S6	0.22	2.5	89.0%	S22	0.40	2.5	89.0%
S7	0.22	2.0	89.0%	S23	0.40	2.0	89.0%
S8	0.22	1.5	89.0%	S24	0.40	1.5	89.0%
S9	0.55	∞	44.5%	S25	0.30	∞	44.5%
S10	0.55	2.5	44.5%	S26	0.30	2.5	44.5%
S11	0.55	2.0	44.5%	S27	0.30	2.0	44.5%
S12	0.55	1.5	44.5%	S28	0.30	1.5	44.5%
S13	0.22	∞	44.5%	S29	0.40	∞	44.5%
S14	0.22	2.5	44.5%	S30	0.40	2.5	44.5%
S15	0.22	2.0	44.5%	S31	0.40	2.0	44.5%
S16	0.22	1.5	44.5%	S32	0.40	1.5	44.5%

Figure captions

Figure 1. Schematic diagram of breakage model with the combination of replacement and cluster method

Figure 2. Principal stress ratio and void ratio versus vertical strain from biaxial tests on: dense specimens with d_{50}=0.55 mm ((a) and (b)); dense specimens with d_{50}=0.22 mm ((c) and (d)); loose specimens with d_{50}=0.55 mm ((e) and (f)); loose specimens with d_{50}=0.22 mm ((g) and (h))

Figure 3. Effect of particle size on the peak and residual principal stress ratio of dense specimens (a) and loose specimens (b) (note that (a) and (b) share the same legend)

Figure 4. Particle displacement field and crushed particles for test S2 (a), S3 (b) and S4 (c)

Figure 5. Particle displacement field and crushed particles for test S6 (a), S7 (b) and S8 (c)

Figure 6. Particle displacement field and crushed particles for test S10 (a), S11 (b) and S12 (c)

Figure 7. Evolution of particle breakage ratio ((a) to (d)) and bond breakage ratio ((e) to (h)) in biaxial tests

Figure 8. Crushed particles at different loading strains in test S8 at 1% (a); 3% (b); 10% (c); 15% (d)

Figure 9. Particle size distribution of dense crushable specimens at different vertical strains: (a)S2 and S6; (b) S3 and S7; (c) S4 and S8

Figure 10. Evolution of void ratio inside shear band in biaxial tests with dense specimens for: tests S1 to S4 with d_{50}=0.55 mm (a); tests S5 to S8 with d_{50}=0.22 mm (b)

Figure 11. Evolution of coordination number in test S1 (a) and test S3 (b)

Figure 12. Probability density functions of friction utilization ratios at peak state for: tests S1 to S4 with d_{50}=0.55 mm at dense state (a); tests S5 to S8 with d_{50}=0.22 mm at dense state (b); tests S9 to S12 with d_{50}=0.55 mm at loose state (c); tests S13 to S16 with d_{50}=0.22 mm at loose state (d)

Figure A1: (a) Equivalent area of a particle; (b) grain size distribution of soil samples; (c) and (d) comparison of the results of biaxial tests from experiments and DEM simulations

Figure 1

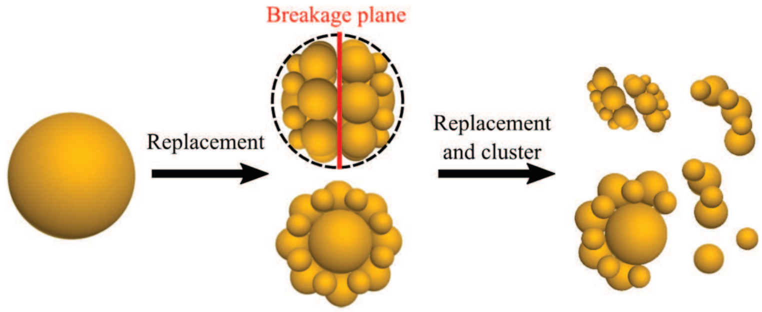

Figure 2

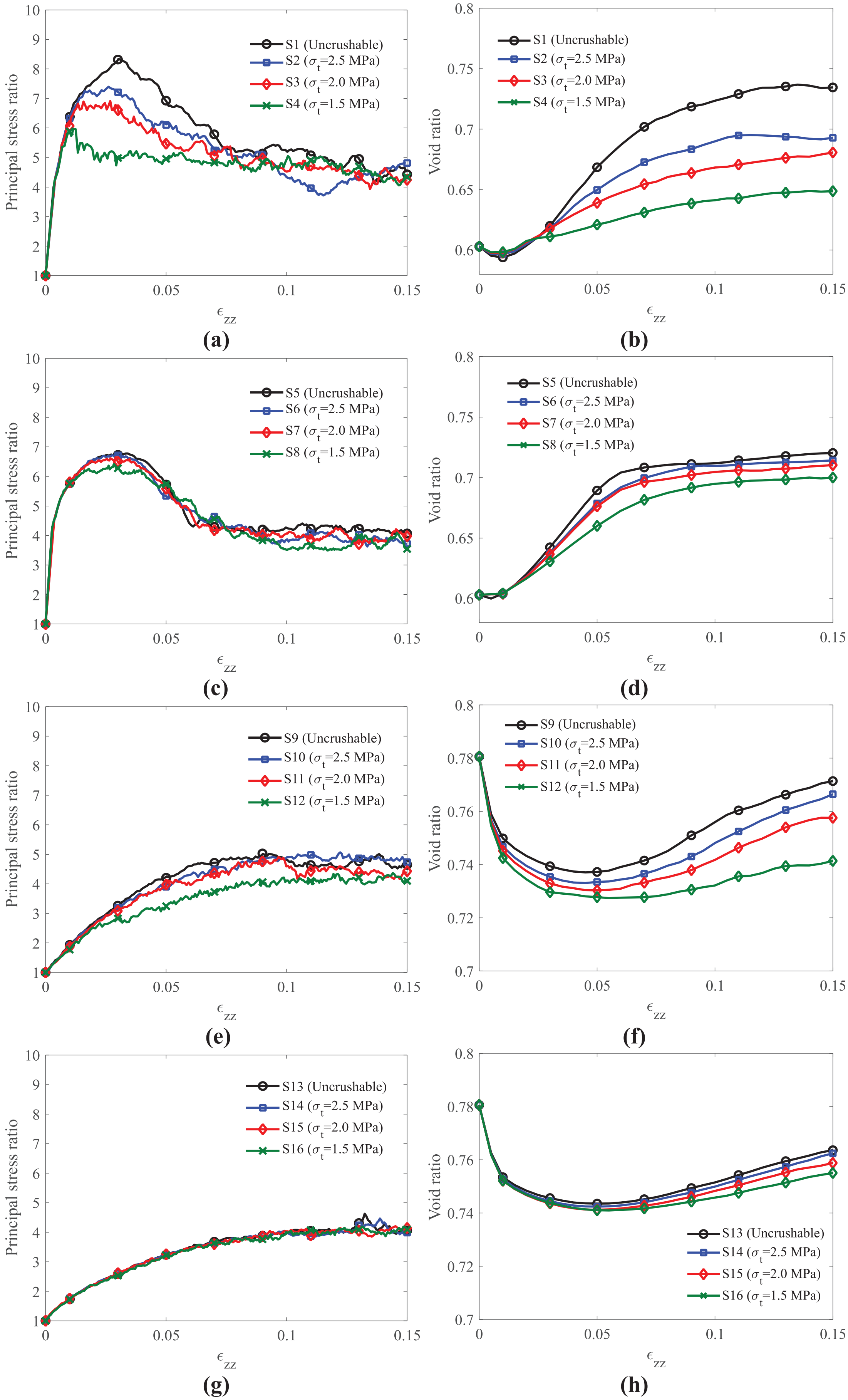
Principal stress ratio
Void ratio
ϵzz
S1 (Uncrushable)
S2 (σt=2.5 MPa)
S3 (σt=2.0 MPa)
S4 (σt=1.5 MPa)
(a)
(b)
S5 (Uncrushable)
S6 (σt=2.5 MPa)
S7 (σt=2.0 MPa)
S8 (σt=1.5 MPa)
(c)
(d)
S9 (Uncrushable)
S10 (σt=2.5 MPa)
S11 (σt=2.0 MPa)
S12 (σt=1.5 MPa)
(e)
(f)
S13 (Uncrushable)
S14 (σt=2.5 MPa)
S15 (σt=2.0 MPa)
S16 (σt=1.5 MPa)
(g)
(h)

Figure 3

Click here to access/download;Figure;Figure_ 3.eps

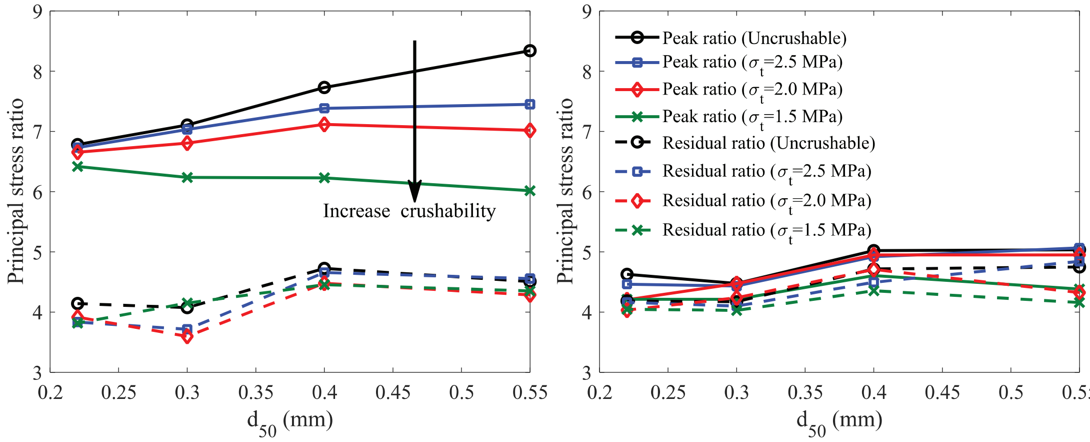

(a) **(b)**

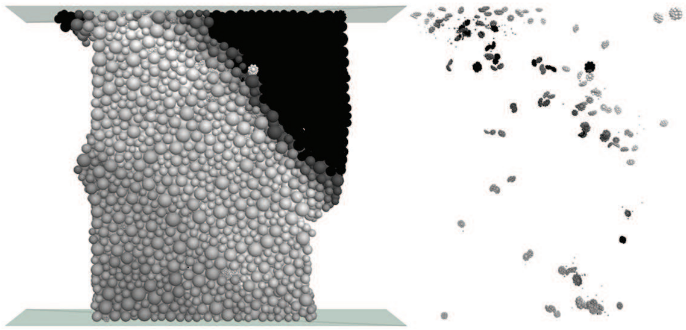
(a)

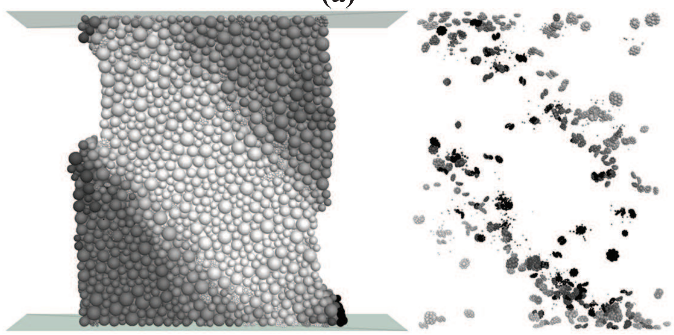
(b)

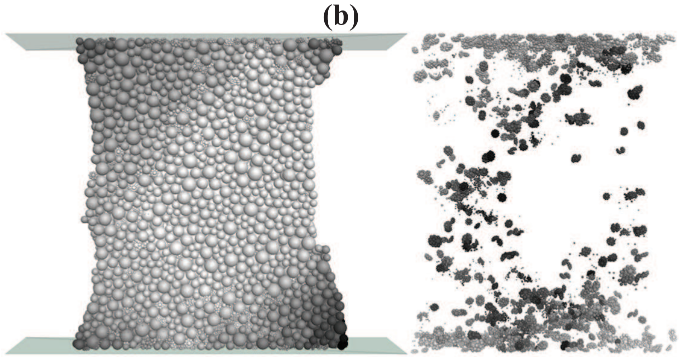
(c)

Figure 5

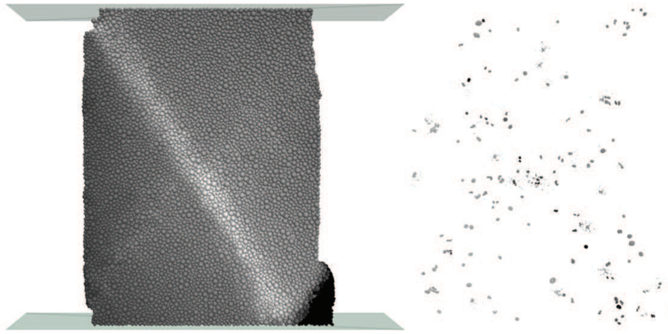

(a)

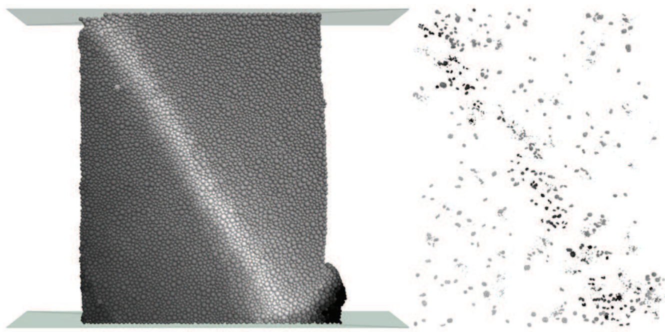

(b)

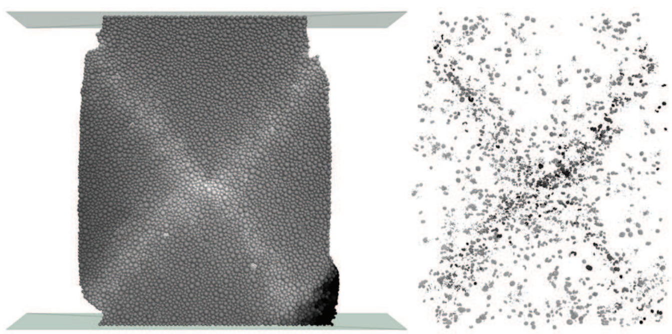

(c)

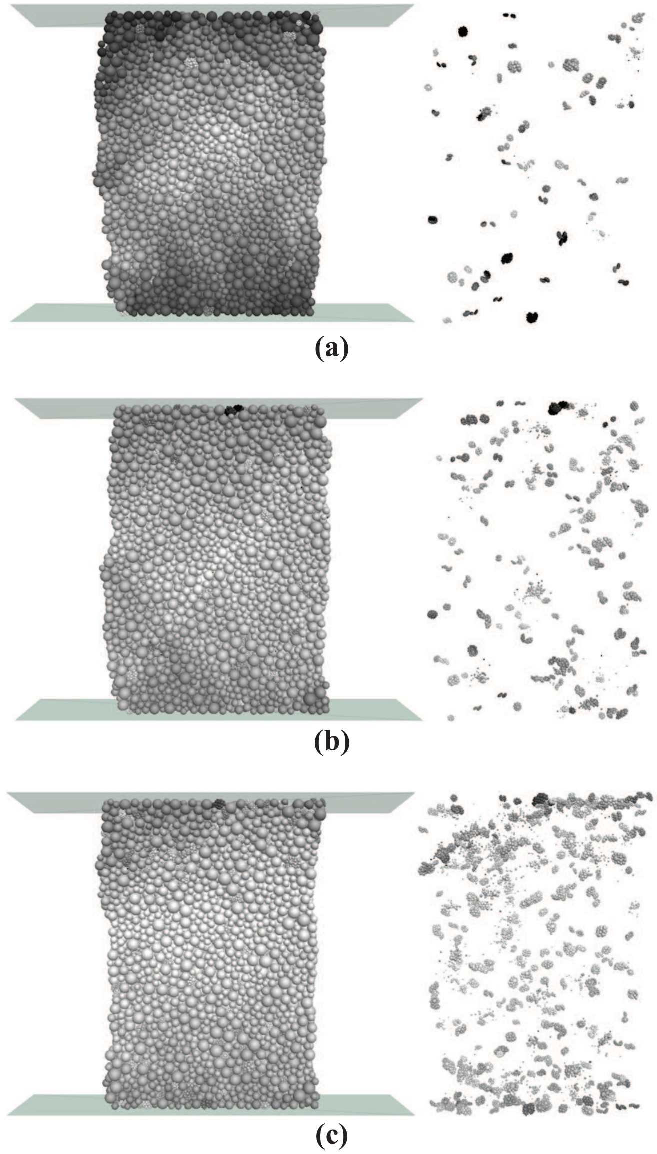
(a)
(b)
(c)

Figure 7

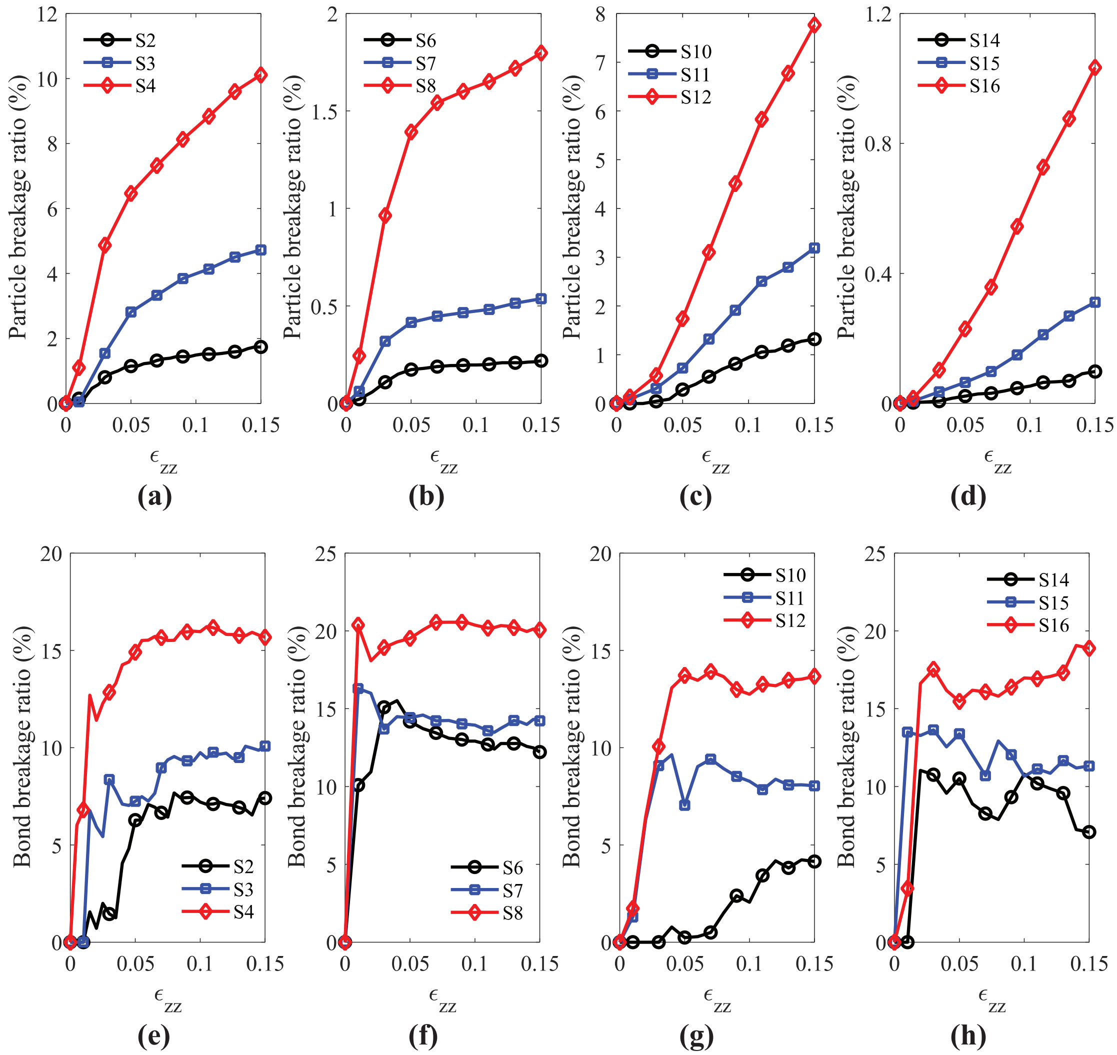
Particle breakage ratio (%)
S2
S3
S4
(a)
S6
S7
S8
(b)
S10
S11
S12
(c)
S14
S15
S16
(d)
Bond breakage ratio (%)
(e)
(f)
(g)
(h)
ϵ_{zz}

Figure 8 Click here to access/download;Figure;Figure_ 8.eps

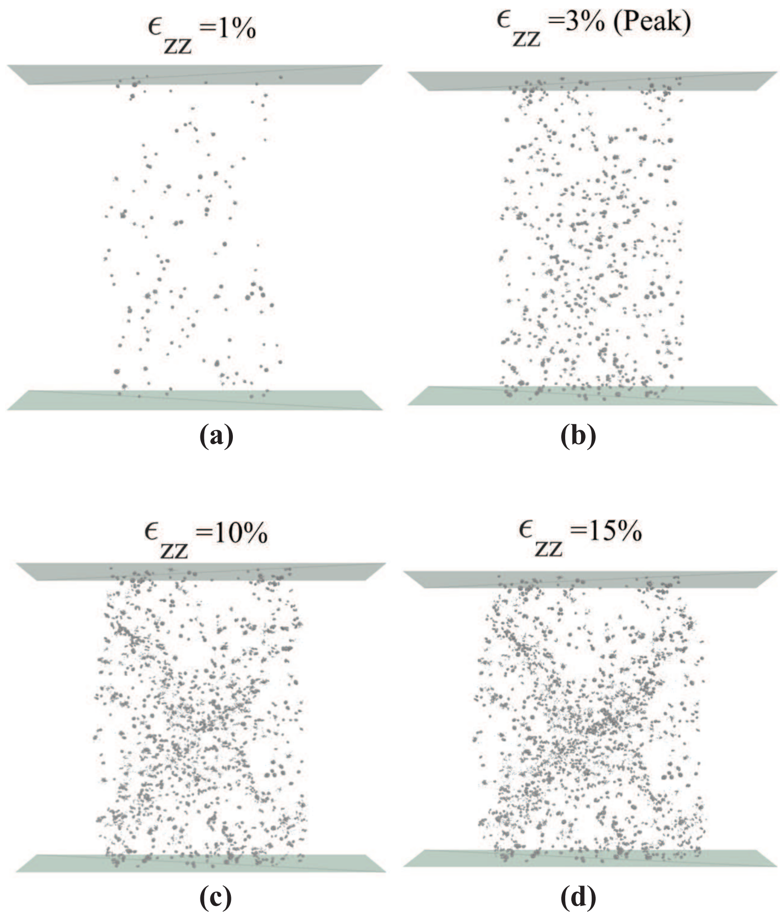

Figure 9

Click here to access/download;Figure;Figure_ 9.eps

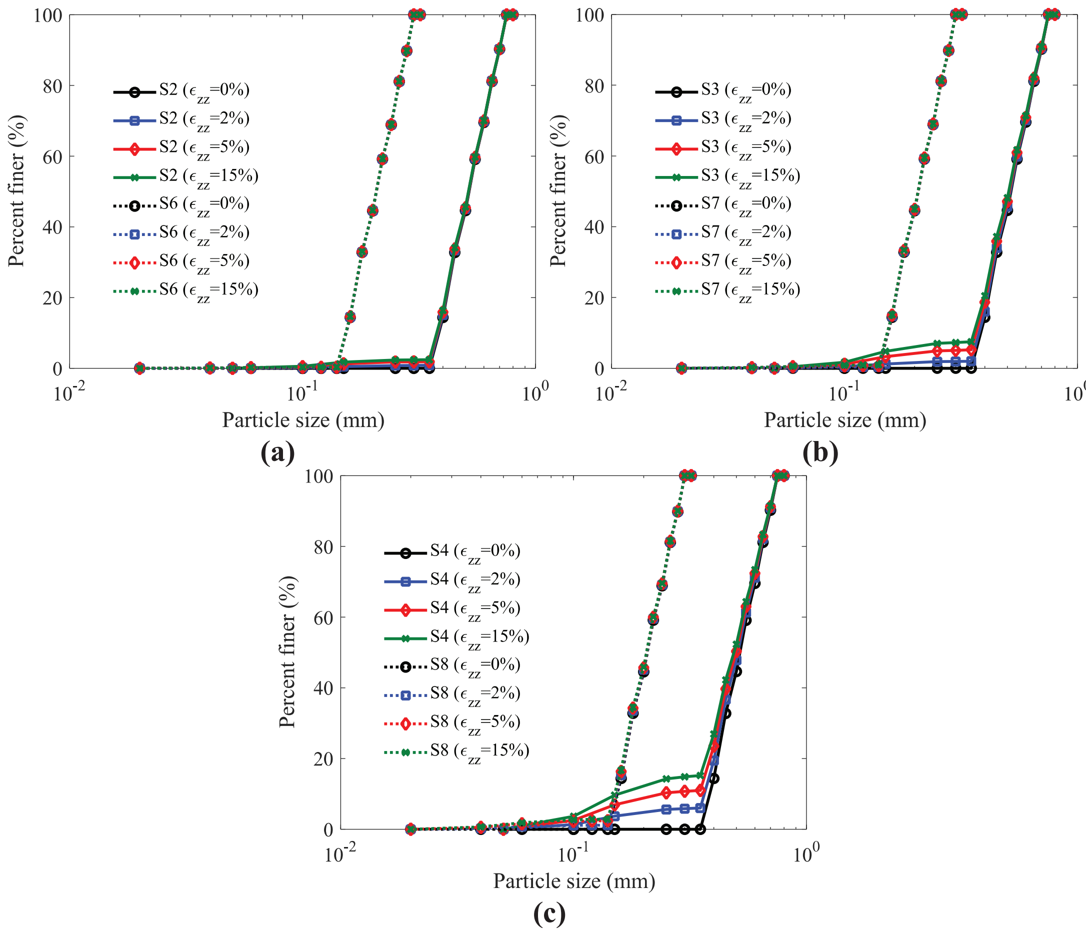

Figure 10

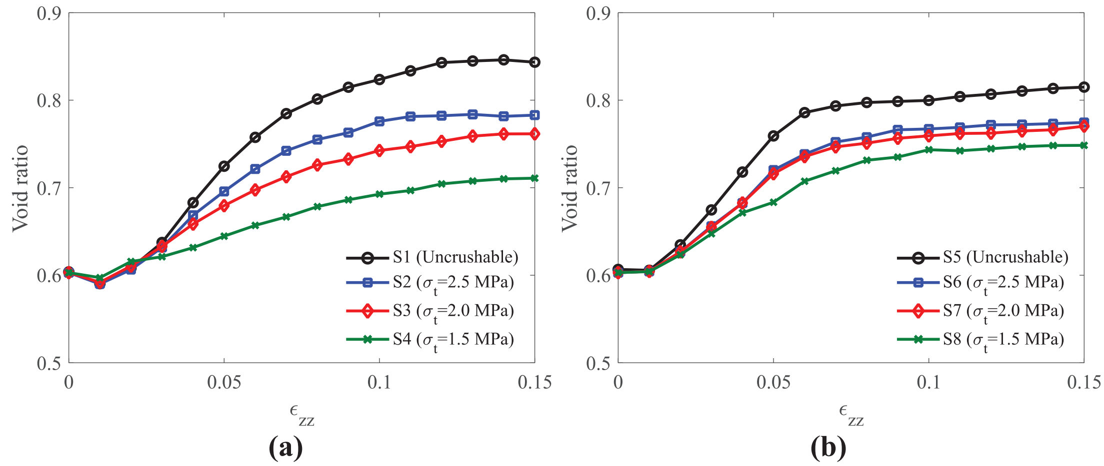

0.9
0.8
0.7
0.6
0.5
Void ratio
0
0.05
0.1
0.15
ϵ_{zz}
S1 (Uncrushable)
S2 (σ_t=2.5 MPa)
S3 (σ_t=2.0 MPa)
S4 (σ_t=1.5 MPa)
(a)
S5 (Uncrushable)
S6 (σ_t=2.5 MPa)
S7 (σ_t=2.0 MPa)
S8 (σ_t=1.5 MPa)
(b)

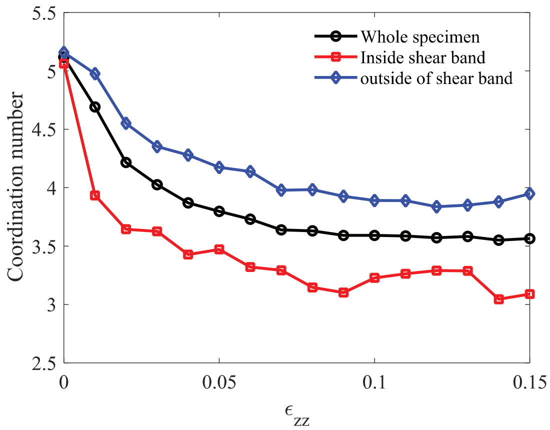
Whole specimen
Inside shear band
outside of shear band
Coordination number
ϵ_{zz}
5.5
5
4.5
4
3.5
3
2.5
0
0.05
0.1
0.15

(a)

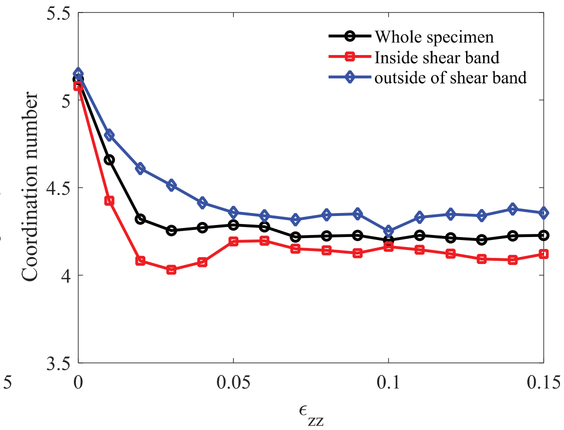
Whole specimen
Inside shear band
outside of shear band
Coordination number
ϵ_{zz}
5.5
5
4.5
4
3.5
0
0.05
0.1
0.15

(b)

Figure 12

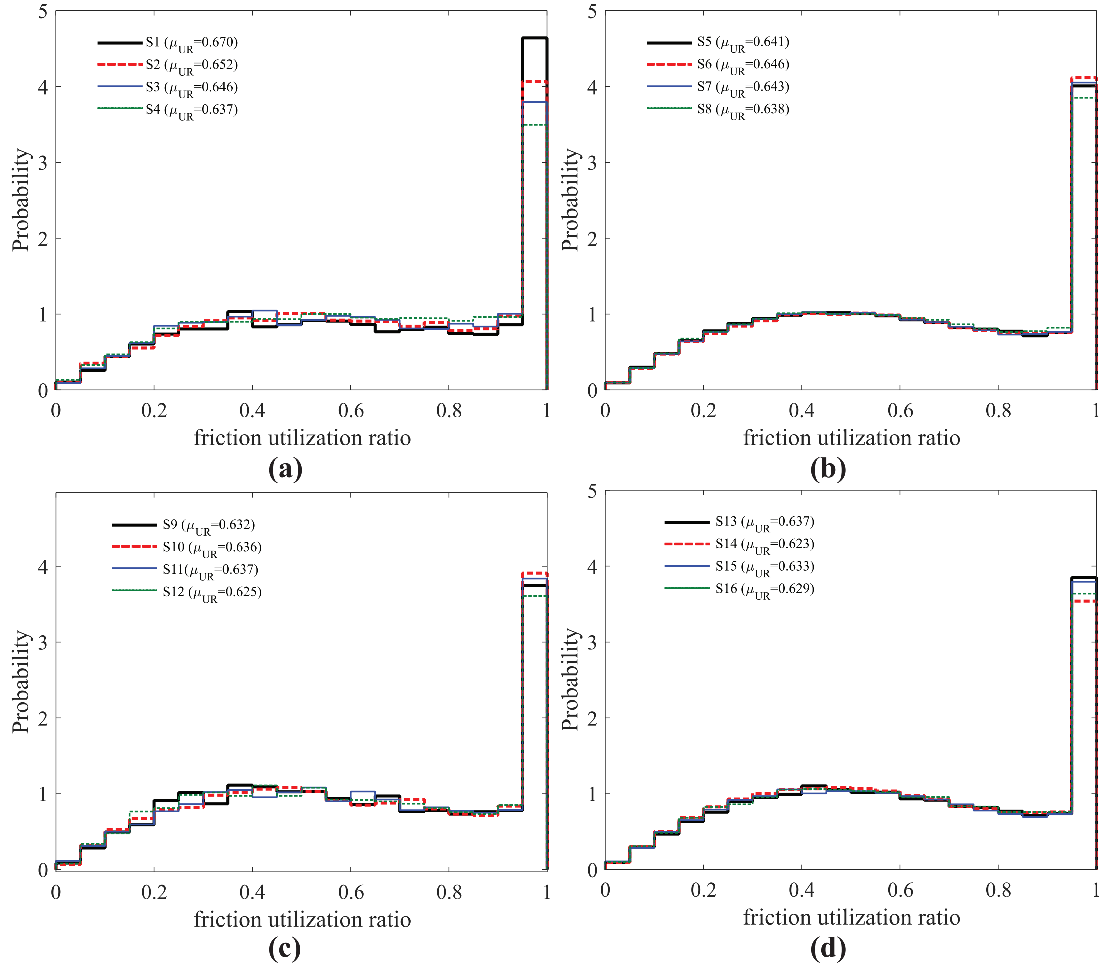

S1 (μ_{UR}=0.670)
S2 (μ_{UR}=0.652)
S3 (μ_{UR}=0.646)
S4 (μ_{UR}=0.637)
Probability
friction utilization ratio
(a)
S5 (μ_{UR}=0.641)
S6 (μ_{UR}=0.646)
S7 (μ_{UR}=0.643)
S8 (μ_{UR}=0.638)
Probability
friction utilization ratio
(b)
S9 (μ_{UR}=0.632)
S10 (μ_{UR}=0.636)
S11(μ_{UR}=0.637)
S12 (μ_{UR}=0.625)
Probability
friction utilization ratio
(c)
S13 (μ_{UR}=0.637)
S14 (μ_{UR}=0.623)
S15 (μ_{UR}=0.633)
S16 (μ_{UR}=0.629)
Probability
friction utilization ratio
(d)

Figure A1

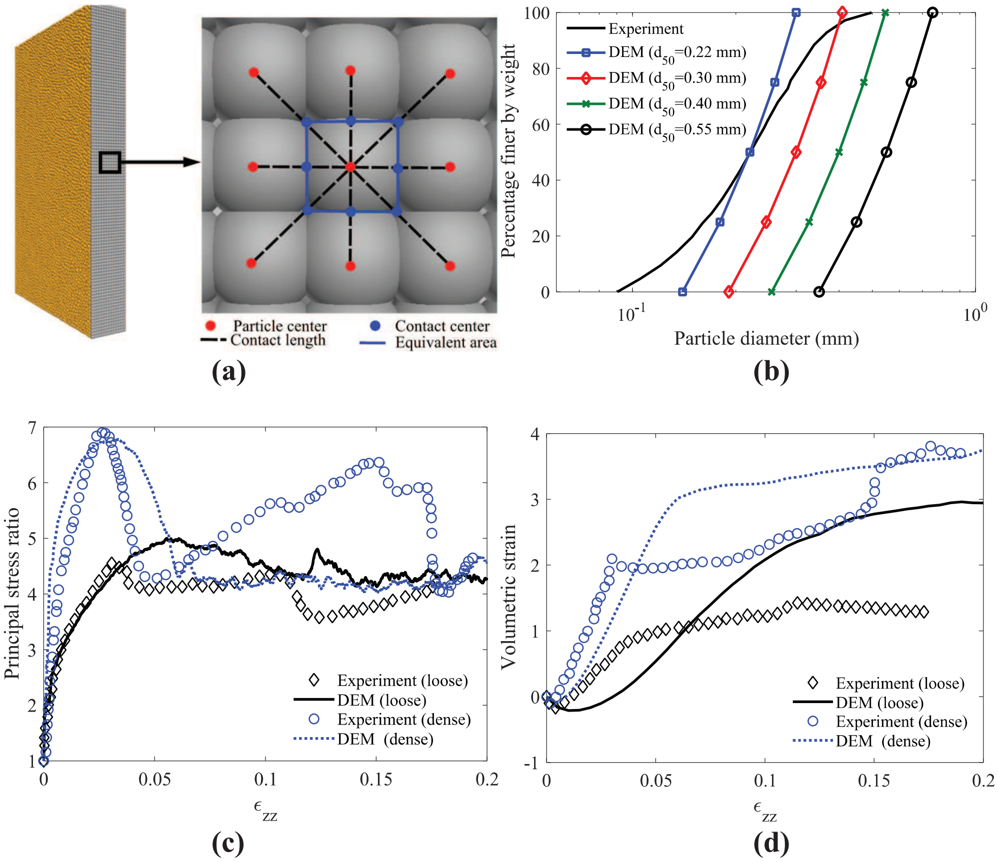

Particle center
Contact center
Contact length
Equivalent area
(a)
Experiment
DEM (d50=0.22 mm)
DEM (d50=0.30 mm)
DEM (d50=0.40 mm)
DEM (d50=0.55 mm)
Percentage finer by weight
Particle diameter (mm)
(b)
Principal stress ratio
Experiment (loose)
DEM (loose)
Experiment (dense)
DEM (dense)
(c)
Volumetric strain
(d)